LASER INTERFEROMETER GRAVITATIONAL WAVE OBSERVATORY
- LIGO -
CALIFORNIA INSTITUTE OF TECHNOLOGY
MASSACHUSETTS INSTITUTE OF TECHNOLOGY

Technical Note	**LIGO-T010075-v3**	**2015/02/17**

Advanced LIGO Systems Design

Advanced LIGO Systems Group
P. Fritschel, D. Coyne, ed.

Distribution of this document:

Systems Acceptance Review Committee

This is an internal working note of the LIGO project

California Institute of Technology
LIGO Project, MS 100-36
Pasadena, CA 91125
Phone (626) 395-2129
Fax (626) 304-9834
E-mail: info@ligo.caltech.edu

Massachusetts Institute of Technology
LIGO Project, NW22-295
Cambridge, MA 02139
Phone (617) 253-4824
Fax (617) 253-7014
E-mail: info@ligo.mit.edu

LIGO Hanford Observatory
127124 North Route 10
Richland, WA 99352
Phone (509) 372-8106
Fax (509) 372-8137
E-mail: info@ligo.caltech.edu

LIGO Livingston Observatory
19100 LIGO Lane
Livingston, LA 70754
Phone (225) 686-3100
Fax (225) 686-7189
E-mail: info@ligo.caltech.edu

http://www.ligo.caltech.edu/

1 Introduction

Advanced LIGO (aLIGO) replaced the three initial LIGO (iLIGO) interferometers with three interferometers using new instrument hardware. The new instruments are designed to provide approximately an order of magnitude better gravitational wave strain sensitivity, and over a wider frequency band.

Initial LIGO (iLIGO) consisted of two interferometers sharing the same vacuum system at the LIGO Hanford Observatory, LHO, (one 4 km long, H1, and one 2 km long, H2) and one (4 km long, L1) interferometer at the LIGO Livingston Observatory, LLO. The original plan was for the aLIGO project to install two 4 km interferometers at the LIGO Hanford Observatory (H1 and H2). Vacuum facility modifications were made to accommodate the two 4 km interferometers at LHO. At the direction of the National Science Foundation (NSF), the aLIGO project has stored the components and assemblies of the second LHO, folded interferometer (H2). The intent is to offer the H2 interferometer components and assemblies (after re-working them into a non-folded interferometer configuration([3])) to India for installation into a third LIGO Observatory better located for astrophysical source localization.

This document describes the system design and requirements for the Advanced LIGO detectors. This version is a final, "as-built" design document, prepared for the Advanced LIGO Systems Acceptance Review (Feb 2015). Changes in the document since the Final Design Review (FDR) version are listed in the version notes field in the LIGO Document Control Center (DCC) entry for this document. This document presents the Design Description, not any "as-built" deviations or revised expectations. For as-built deviations, see the Systems Acceptance document ([1]).

This document represents the System requirements and top-level system design, i.e. design within the scope of the systems group; This document is not an attempt to summarize the subsystem design decisions and attributes. For a top-level description of the entire aLIGO system, see also the recent aLIGO overview paper ([2]) written by the Systems group for the LIGO Scientific Collaboration (LSC).

2 System Level Requirements

2.1 Strain Noise

The goal sensitivity for the Advanced LIGO detectors is defined in the Project Execution Plan ([4]) and the Advanced LIGO Reference Design ([5]) as: an equivalent (single interferometer) strain noise of 10^{-22} RMS, integrated over a 100 Hz bandwidth centered at the minimum noise region of the strain spectral density.

2.2 Non-Gaussian Noise

The initial LIGO science requirements document ([6]) specified that, at the targeted threshold of sensitivity, the false signal rate (i.e., triple coincidences not due to astrophysical sources)

should be held to less than 0.1 events per year. For Advanced LIGO, we would like to reach a rate at least as low as this, if not lower. However, there are few if any places where this can really be quantitatively factored into the hardware design. Lessons learned from initial LIGO about potential sources of glitches must be incorporated into the designs. In addition, general mechanical design rules are followed, such as limiting stress concentrations and avoiding bolts in sensitive locations.

2.3 Availability

The detector availability goals for initial LIGO are also adopted for Advanced LIGO; these are [6]:

- Single interferometer operation: 90% availability (annually integrated), minimun lock duration of 40 hours
- Double coincidence operation (LLO interferometer with either LHO interferometer): 85% availability, averaged annually
- Triple coincidence operation: 75% availability, averaged annually

For comparison, the corresponding duty cycles over the last 30 days of initial LIGO's S5 run were: 88%, 85.2% and 76.3% for H1, H2 and L1 single operation, respectively; 73.8% for LLO-LHO double coincidence; 69.1% for triple coincidence. These numbers represent significant improvement over the course of the run; the duty cycles averaged over all S5 are 10-15% lower than these.

A heuristic approach to an availability analysis ([7]) suggests 80% duty cycle for single interferometer operation (likely an upper bound). Operational experience on a complex, one-of-a-kind system such as aLIGO is needed before confidence is gained in availability estimates.

2.4 Environmental Sensing

The detector environment will be monitored with initial LIGO's Physics Environment Monitoring (PEM) system. No additional monitoring functions are planned at this time. Future environmental sensing upgrades might involve (a) deploying more vibration sensors for the ground and vacuum equipment, for the purpose of subtraction of Newtonian noise from the data stream, and (b) the addition of ground (or seismic isolation system first stage) tilt sensors for use in feedforward correction of active seismic isolation control.

2.5 Calibration and Data Acquisition

Errors in the interferometer response function degrade the ability to detect gravitational waves and the ability to measure source properties of detected signals. Calibration accuracy is naturally more important for source parameter extraction than for detection. We have set the calibration accuracy requirements at 5% in amplitude and 16sec in timing, over 2 confidence

levels. This is consistent with requirements for detection of strong binary black-hole signals ([8]).

The gravitational-wave data channel(s) will be recorded at a rate of 16384 samples/sec (same as initial LIGO), with a bandwidth of 7400 Hz or greater and a precision sufficient for the dynamic range of the channel. Collaborative channels that monitor the instrument (dozens of non-GW degrees-of-freedom) and its environment (the PEM subsystem) will also be recorded so that they can be used to distinguish instrumental artifacts from potential GW signals.

3 System Design

The Advanced LIGO configuration, shown in Figure 1, is a Michelson interferometer with Fabry-Perot arm cavities, and both power recycling and signal recycling (i.e., the initial LIGO configuration, with the addition of signal recycling). There is both an input mode cleaner (as in initial LIGO) and output mode cleaner (new with Advanced LIGO), the latter being required for the gravitational wave (GW) readout. Top level design parameters are given in Table 1.

Parameter	*Value*	*Comments*
Arm length	3994.5 m	
Arm cavity finesse	450	see Sec. 3.7
Laser type and wavelength	Nd:YAG, $\lambda = 1064\,\mathrm{nm}$	
Input power (@ PRM)	5 – 125 W	
Beam polarization	linear, horizontal	in arms & RCs
Test mass material	Fused silica	see Sec. 3.8
Test mass size & mass	$\phi\,34\,\mathrm{cm} \times 20\,\mathrm{cm}$, 40 kg	see Sec. 3.9
Beam radius ($1/e^2$), ITM / ETM	5.3 cm / 6.2 cm	see Sec. 3.5
Radii of curvature, ITM / ETM	1934 m / 2245 m	see Sec. 3.6
Beamsplitter size & mass	$\phi\,37\,\mathrm{cm} \times 6\,\mathrm{cm}$, 14 kg	
Michelson (Schnupp) asymmetry	8 cm	see Ref. [9]
Input mode cleaner length & finesse	32.9 m (round trip), 500	
Recycling cavity lengths, PRC / SRC	57.6 m / 56.0 m	

Table 1: Parameters of the Advanced LIGO interferometers. Exact values for all the interferometer lengths and precise optics dimensions are found in Ref. [10]. The full set of cavity parameters – mirror reflectivities, beam sizes, etc. – are found in Ref. [11]. PRC, power recycling cavity; SRC, signal recycling cavity.

3.1 Modes of operation

Two features of the interferometer design provide flexibility so that, unlike initial LIGO, the detectors can be operated in different modes with good broadband GW sensitivity, or sensitivity targeted to specific frequency bands. The two features are: tuning of the signal

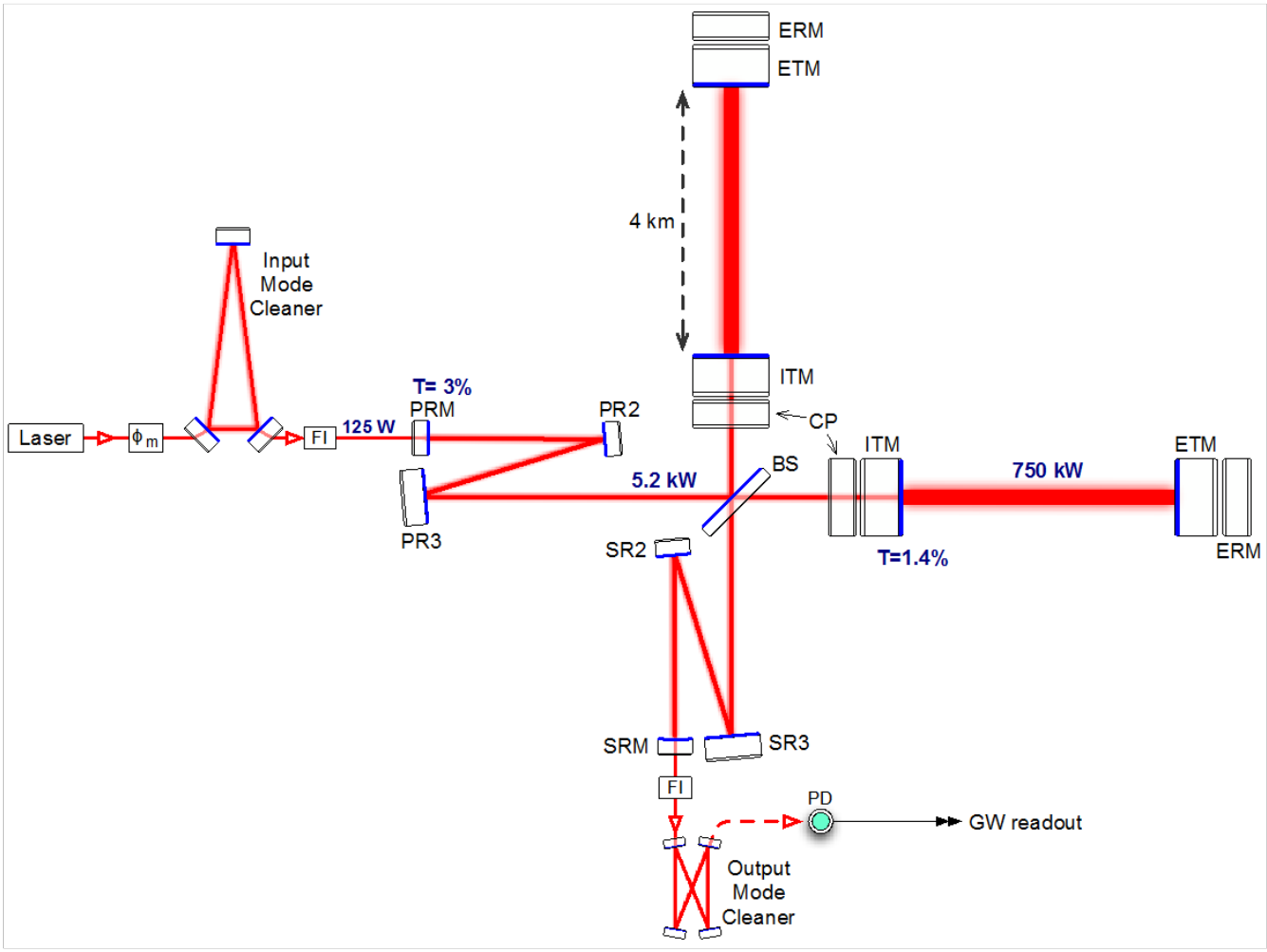

Figure 1: Advanced LIGO interferometer configuration. ETM, end test mass; ITM, input test mass; BS, 50/50 beamsplitter; CP, compensation plate; ERM, end reaction mass; PRM, power recycling mirror; SRM, signal recycling mirror; PR2/3, power recycling cavity mirror 2/3; SR2/3, signal recycling cavity mirror 2/3; FI, Faraday isolator; $\phi_{\rm m}$, phase modulation; PD, photodetector. The power levels shown correspond to full-power operation; the interferometers can also be operated at much lower power with good strain sensitivity.

recycling cavity (SRC); the trade-off between low frequency and high frequency noise with laser power.

Advanced LIGO's sensitivity improvement at frequencies below $\sim 200\,\mathrm{Hz}$ are mostly the result of the much better seismic isolation and test mass suspensions. We intend to capitalize on these hardware improvements as rapidly as possible by taking a staged approach to the interferometry. Our approach is to begin operating the interferometer at a modest power level with broadband signal recycling. The operating power would then be increased in the broadband mode, up to the maximum power available depending on the frequency band one wants to target, and the difficulties handling high power. Tuned operation of the signal cavity could follow (e.g., optimized for binary neutron star inspiral), as informed by results.

Strain noise spectra for these modes are shown in Fig. 2 and operating parameters are given in Table 2.

Low power mode In this mode there is broadband signal recycling (i.e., zero detuning of the signal recycling cavity). This mode is expected to be significantly easier to control than those where the signal cavity is tuned away from zero frequency. This mode could be run with different input powers, starting with low power. At high power, the sensitivity to binary neutron star inspirals is almost as good as can be achieved by specifically tuning for them.

BNS optimized mode This is a full power mode with the SRC tuned to optimize sensitivity to NS-NS inspirals. We have however fixed the SRM transmission at 20%, which is a bit higher than the optimum for NS-NS sensitivity, as a compromise with the broadband case (the difference is less than 0.4%).

Nominal mode This is the canonical broadband (zero detuned SRC), full power mode with the SRM transmission set at 20%).

Mode	*NS-NS Range*	*BH-BH Range*	P_{in}	T_{SRM}	ϕ_{SRC}	h_{RMS}, 10^{-23} (*band*)
Low power	160 Mpc	1.70 Gpc	25 W	35%	0 deg.	5.5 (85 - 185 Hz)
BNS optimized	210 Mpc	1.75 Gpc	125 W	20%	16 deg.	2.7 (200 - 300 Hz)
Nominal	190 Mpc	1.71 Gpc	125 W	20%	0 deg.	3.5 (230 - 330 Hz)

Table 2: Sensitivities for the operational modes described above, and shown in Fig. 2; the last column gives the minimum RMS strain noise in a 100 Hz band

Baseline mode. Due to its good wideband sensitivity and relative simplicity of operation, the non-detuned signal-recycled configuration is established as the baseline mode.

3.2 Signal Recycling

Signal recycling is included in the design because it offers advantages in sensitivity and in practical operations. For the maximum input and stored arm powers, a non-signal recycled

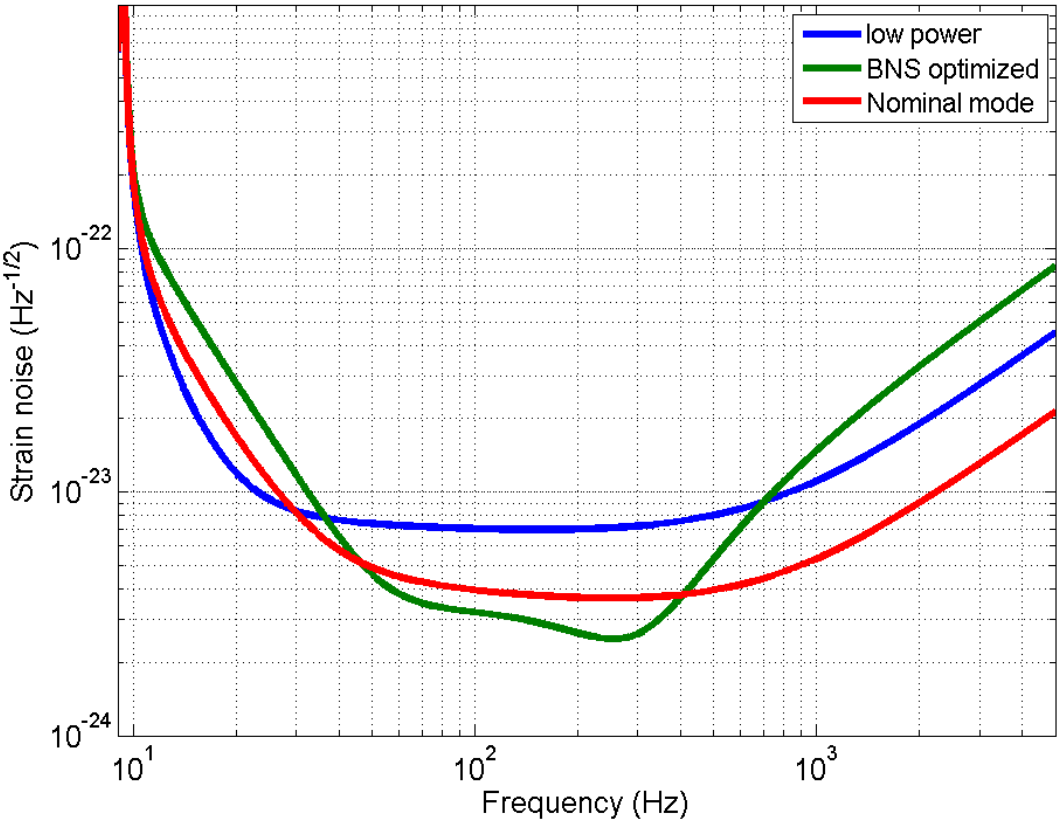

Figure 2: Advanced LIGO strain noise spectrum for three operational modes. The feature at 500 Hz is the (unresolved) fundamental vibrational mode of the test mass suspension fibres. See text for description of the modes.

interferometer could in principle reach a NS-NS inspiral range that is only about 10% lower than the signal-recycled version, but the power recycling cavity (PRC) would need to support about 10 times more power in this case and the losses in the PRC would need to be kept extremely low. And of course signal recycling is needed to really optimize sensitivity above a couple of hundred Hertz.

The Advanced LIGO interferometer will be built at least initially with fixed-transmission signal recycling mirrors (SRM). This means that to achieve the best narrow-band sensitivity above $\sim$1 kHz, the SRM would need to be changed for one with a lower transmission. A later upgrade could implement a variable-transmission SRM.

3.3 Laser and Input Optics

The laser wavelength is specified to be 1064 nm, as in initial LIGO. As mentioned in Sec. 3.1, we plan on operating the interferometers with a range of input power levels. The range of laser power that can be delivered to the interferometer, at the power recycling mirror, is specified to be 5 W – 125 W. Over this range of powers, the laser and all other interferometer subsystems must be capable of operating in science mode and meeting their performance requirements[1]. For lock acquisition, it will be possible to reduce the power to 100 mW.

As in initial LIGO, the laser itself is part of a pre-stabilized laser (PSL) system, and the output of the PSL passes through various input optics (IO) that condition the beam before it impinges on the power recycling mirror (PRM). In order to deliver 125 W at the PRM, the PSL output power is required to be $\geq$ 165 W in a single-frequency, TEM_{00} mode.

The input optics are very similar to initial LIGO in function, but designed for higher power. Outside of the vacuum, the IO contains a variable attenuator to control the laser power level, and phase modulators that generate RF sidebands used for interferometer global control. Inside the vacuum, the IO contains a triangular, suspended-mirror mode cleaner that provides a directionally-stable fundamental mode beam and an intermediate frequency reference; a Faraday isolator between the mode cleaner and the PRM; and optics to mode-match the beam to the interferometer mode. Remote tuning of this mode-matching might be considered as a future upgrade to the input optics.

3.4 GW Channel Readout

Readout of the gravitational-wave channel will be done using an output mode cleaner in conjunction with homodyne, or DC, detection, in part because of its compatibility with the use of squeezed light. This readout scheme was successfully implemented for Enhanced LIGO (eLIGO ([12]).

The output mode cleaner will filter out non-TEM_{00} mode carrier power, and any power in RF modulation sidebands, so that only the carrier TEM_{00} mode power is detected. This greatly reduces the power on the detectors, lowering the noise with only a small reduction in signal.

Homodyne (DC) readout was adopted over heterodyne (RF) readout in 2003 ([13]) due to its intrinsically lower sensing noise and reduced sensitivity to laser and technical noises. The

[1] some performance requirements, such as laser power noise, will depend on the laser power

sensing noise comparison between the two types of readout is made in Ref. [14], and a review of technical considerations, including comparison data from the 40m interferometer, can be found in Ref. [15]. A possible future upgrade is to implement balanced homodyne readout ([16]).

3.5 Beam Sizes

The beam sizes on the test masses will be 5.3 cm on the ITMs and 6.2 cm on the ETMs ($1/e^2$ intensity radius). They are made large (compared to initial LIGO) in order to reduce test mass thermal noise by averaging over more of the mirror surface. The dominant noise mechanism here is mechanical loss in the dielectric mirror coatings, for which the displacement (amplitude) noise scales as 1/(beamsize). Close behind is thermo-optic noise in the coatings, which scales as $(\text{beamsize})^{-1/2}$.

The thermal noise reduction with increased beam size has to be balanced against increased aperture loss and decreased mode stability. The slightly asymmetric design of the arm cavity takes advantage of the fact that the ETMs are more important for reducing thermal noise because their coatings are thicker (2-3 times as thick as the ITMs). Therefore we can achieve essentially the same level of thermal noise and mode stability by making the beam larger on the ETM and smaller on the ITM. This has the advantage of reducing aperture loss in the beamsplitter and recycling cavities. For comparison, a symmetric design, with 6.2 cm beams on all arm cavity mirrors, would have about 4% lower test mass thermal noise at 100 Hz than the chosen design.

The chosen design has fairly low aperture loss in the arms, 2–3 ppm on the ETMs. While this could arguably be allowed to be larger, doing so would push the arm cavities further toward the mode stability edge (the design has $g_1 g_2 = 0.845$, where the stable zone is $0 \leq g_1 g_2 \leq 1$). Tighter tolerances would be needed on the arm mirror radii of curvature; larger-scale polishing distortions would become important. We are therfore reluctant to go further in this direction without having some experience making and operating cavities in this regime.

3.6 Arm Cavity Radii of Curvature

The chosen mirror beam sizes can be achieved with either of two designs: a nearly-planar cavity or a nearly-concentric one. Our choice is made from consideration of optical torques in the arm cavities, which become important at the Advanced LIGO power levels. The analysis of optical torques given in Ref. [17] shows that there is a preference for the nearly concentric design. In this case, the torsional mode with the higher optical stiffness is statically stable, whereas it would be statically unstable for a near planar design.

The near-concentric design has a smaller arm cavity waist ($\omega_0 = 1.3$ cm) by a factor of 3.5. This does lead to larger phase noise from beam tube residual gas fluctuations, but this is still a small noise term. We're not aware of any other disadvantages of the smaller waist.

3.7 Arm Cavity Finesse

With signal recycling, the quantum noise-limited strain sensitivity is more-or-less independent of the arm cavity finesse, and the finesse choice is guided by practical considerations. Generally these argue for a higher arm cavity finesse than in initial LIGO. PRC loss favors higher arm finesse (smaller recycling gain) and SRC loss favors lower arm finesse. A deficient PRC gain can be compensated by higher input power to reach a target stored arm power level. However SRC loss would be to be compensated by a higher stored power level, which increases thermal distortion and radiation pressure concerns. With the ultra-low absorption FS test masses, bulk absorption is not an issue, and so there is no motivation to keep power low in the ITM substrates. A trade-off analysis ([18]) of the competing technical considerations (e.g. substrate absorption, coating thermal loss, coupling of auxiliary degrees-of-freedom, DC readout, lock acquisition, high frequency tuned configuration) led to an arm finesse design value of 450.

3.8 Core Optic Material

All core optics, included the test masses, will be made of fused silica. In the early 2000's sapphire was also considered for the test mass material. The pros and cons of both materials were examined in detail, and at the end of 2004 an evaluation committee concluded that fused silica was the better choice. This decision is summarized in Ref. [19], and further technical details can be found in Ref. [20]. Essentially, there was no clear overall performance advantage for either material, whereas manufacturing and processing issues favored fused silica.

There are several types and grades of fused silica from which to choose. Low mechanical dissipation is important for the test masses, but all types of fused silica appear to have sufficiently low loss that this is not a discriminator. For those optics whose substrate is in an interferometer cavity – input test masses, beamsplitter, and compensation plates – the important properites are optical absorption and homogeneity. For the ITMs and BS, initial LIGO uses a low-absorption grade (Heraeus 312), which has 3-4 ppm/cm of absorption at 1064 nm. Advanced LIGO will instead use the ultra-low-absorption Heraeus Suprasil 3001 material for the ITMs, BS, and CPs. The absorption level for this material has been measured to be < 0.2 ppm/cm. This will ensure that the power absorbed in the bulk is negligible compared to that absorbed in the coatings.

The other core optics do not have such stringent materials requirements, and we do not specify their fused silica type at the systems level.

3.9 Test Mass Size

The mass of the fused silica test masses is 40 kg, four times larger than in initial LIGO. The benefit of the increased mass is to reduce radiation pressure noise (scales inversely with the mass).

The choice of aspect ratio is explored in Ref. [21]. It should be noted that while this considers thermal noise of the substrate as a function of aspect ratio, the dominant noise due to the optical coatings is not treated, as at the time there was no coating noise model that included the finite test mass size. A more recent formulation ([22]) of coating thermal noise

which considers finite sized optics shows that our aspect ratio the correction is very small. Consideration of Parametric Instability modes was also not considered in the trade-off analysis of aspect ratio.

3.10 Test Mass Coatings

The traditional multi-layer dielectric mirror coating contains alternating layers of low-index and high-index thin film materials, each with an optical thickness of 1/4-wavelength. For the Advanced LIGO test masses, however, there are a couple of reasons to deviate from the standard 1/4-wave design. First, the coating thermal noise may be reduced by using a different layer thickness ratio, if one of the layer materials has higher mechanical loss than the other. Second, we require the coatings to be dichroic, with specific transmission values at 1064 nm and 532 nm (see Sec. 3.18) that require a non-1/4-wave design. (Note that while the probe beams used with the Hartmann Wavefront Sensor (WFS) (see Sec. 3.17) rely upon optical characteristics of the TM coating at other wavelengths, these considerations drove the consideration of the HWS probe beam, not the TM coating design.)

The critical properties of the coating materials are low optical absorption, low scatter, and low mechanical loss. Research on various materials has yielded a coating formulation that reduces mechanical loss, and maintains the low absorption and scatter of traditional coatings: silicon-dioxide for the low-index material, and tantalum pentoxide doped with 25% titanium dioxide for the high-index material ([23]). While the doped-tantala mechanical loss is still several times higher than that of silica, the overall mechanical loss is about 40% lower than the non-doped coatings used in initial LIGO.

The coating components are thus specified to the coating vendor to be silica and doped-tantala. Optical transmission values are also specified (see Sec. 3.12). The specific layer thicknesses are not specified (these are better determined by the vendor), but they are directed to make a best effort at minimizing thermal noise. The dichroic nature does push the coating layer thicknesses in a direction that reduces thermal noise. We estimate that the coating design will have several percent lower thermal noise (in amplitude) than a 1/4-wave design that meets the 1064 nm transmission specifications.

The potential benefits of a gold coating on the barrel of the test masses have been investigated in some detail, concluding with the decision to not gold-coat the barrels. This conclusion was based on the following assessments:

- Acoustic mode damping. A gold barrel coating could mechanically damp test mass acoustic modes involved in potential parametric instabilities (see Sec. 3.19). However, it was found that to limit the increase in thermal noise that such a coating would introduce, it would have to be made so thin that it would not provide significant mode damping.
- Electro-static charge control. A gold barrel coating could help control charge buildup on the test mass, however there is no clear scenario where it could help. The primary areas to be concerned about static charge are on the faces of the test mass, and at the areas adjacent to the earthquake stops (see Sec. 3.20).

- Thermal compensation. A gold barrel coating would prevent heat flow out the barrel, and might provide some thermal distortion/compensation benefit. Analysis of thermal compensation with and without the barrel coating showed no clear benefit to either case ([24]).

3.11 Interferometer Optical Losses

Optical loss in the arms limits the power build-up and thus the shot-noise sensitivity, for a given input power. The goal for round-trip arm cavity loss is 75 ppm (includes scatter and absorption, and ETM transmission). This is a factor of 1.5-2 times lower than observed in the initial LIGO arm cavity mirrors. The design budget breakdown for arm cavity loss ([25]) is:

ETM transmission	6 ppm
Scatter from microroughness (0.16 nm rms)	2×5 ppm
Scatter from point defects	2×5 ppm
Cumulative contamination scattering	2×4 ppm
Surface absorption	2×0.5 ppm
Cumulative contamination absorption	2×1 ppm
Surface distortion (≈ 0.5 nm rms)	2×18 ppm
Finate aperture diffraction loss	2×1 ppm
Total	**75 ppm**

The goal for round-trip loss in the power recycling cavity (not including the arms) is 1000 ppm, which corresponds to 5% of the loss from the arm cavities ($4 \cdot 75\,\mathrm{ppm}/T_{\mathrm{ITM}} = 2.1\%$). For the signal recycling cavity, the round-trip loss goal is 2000 ppm, or 1% of the SRM transmission. In the most sensitive frequency region, around a couple of hundred Hz, this level of loss would degrade the strain sensitivity by about 5%.

Absorption. While coating and bulk absorption are very small compared to the total optical losses, achieving low absorption levels is critical to high power operation, due to the thermal distortions they can produce. By far most power is absorbed in the test mass reflective coatings. For these, the absorption requirement is 0.5 ppm or less.

Bulk absorption in the core optic substrates is minimized by using ultra-low absorption fused silica where appropriate (see Sec. 3.8). Reflective surfaces for non-TM core optics are specified at an absorption level of 1 ppm or less. The expected levels of absorbed power, for 800 kW in each arm cavity, and assuming 0.5 ppm absorption on all HR surfaces and < 0.2 ppm/cm in the bulk, are:

Test mass HR surface	400 mW
ITM substrate	< 22 mW
CP substrate	< 15 mW
BS 50-50 surface	2.8 mW
BS substrate	< 3.9 mW

3.12 Core Optics Parameters

For reference the top level parameters of the core optics are given in Table 3.

Optic	*Dimensions: diam.×thickness*	*Mass*	*Transmission*	ROC	*Beam size* ($1/e^2$ radius)
ITM	34 × 20 cm	40 kg	1.4% (<1%)	1934 m	5.3 cm
ETM	34 × 20 cm	40 kg	5 ppm (∼5%)	2245 m	6.2 cm
CP	34 × 10 cm	20 kg	AR< 50 ppm	flat	5.3 cm
ERM	34 × 13 cm	26 kg	AR< 1000 ppm	flat	6.2 cm
BS	37 × 6 cm	14 kg	50%	flat	5.3 cm
PR3	26.5 × 10 cm	12 kg	< 15 ppm	36.0 m	5.4 cm
SR3	26.5 × 10 cm	12 kg	< 15 ppm	36.0 m	5.4 cm
PR2	15 × 7.5 cm	2.9 kg	250 ppm	-4.56 m	6.2 mm
SR2	15 × 7.5 cm	2.9 kg	< 15 ppm	-6.43 m	8.2 mm
PRM	15 × 7.5 cm	2.9 kg	3.0%	-11.0 m	2.2 mm
SRM	15 × 7.5 cm	2.9 kg	20%	-5.69 m	2.1 mm

Table 3: Parameters of the core optics. ITM: input test mass; ETM: end test mass; CP: compensation plate; ERM: end reaction mass; BS: beam splitter; PR3: power recycling mirror 3; SR3: signal recycling mirror 3; PR2: power recycling mirror 2; SR2: signal recycling mirror 2; PRM: power recycling mirror; SRM: signal recycling mirror. ROC: radius of curvature. The transmission values are for 1064 nm, except for the values in green, which are for 532 nm. Where specified for 'AR', or anti-reflection, the value refers to each of the two surfaces of the optic. The dimensions and masses are rounded-off values, and do not include details such as wedges or bevels. (see Ref. [11]).

3.13 Arm Matching

The two arms of the interferometer must be well matched in order to limit the coupling of laser noise to the GW readout, and to maintain good overlap of the fields in the two arms to preserve signal amplitude. The following requirements for matching of the two arms are set:

Beamsplitter splitting ratio	$\lvert T_{\rm BS} - 0.5\rvert < 0.005$
ITM transmission matching	$T_{\rm ITM}$ matched to < 1%
Arm round trip loss difference	35 ppm
Test mass ROC matching	To within ±10 m, goal of ±3 m

The beamsplitter ratio and the ITM transmission matching are relevant for technical radiation pressure noise (i.e., originating from laser power noise). The required laser power stability is thus calculated assuming a ≈ 1% imbalance in the arm powers ([27], [28]). Laser frequency noise and RF oscillator noise coupling depend on ITM transmission matching and the difference in round trip loss between the arms [27]. The round trip loss difference (35

ppm) is an assumed worst case for the purpose of deriving these noise requirements. The ROC (radius of curvature) matching of the test masses is important for maintaining signal recycling gain and minimizing contrast defect.

3.14 Recycling Cavity Geometry

Both power- and signal-recycling cavities are made to be stable for the fundamental Gaussian modes they support. By *stable* we mean that the fundamental mode of the cavity accrues a non-negligible Gouy phase in a one-way propagation through the cavity. In contrast, the initial LIGO power recycling cavity is marginally stable, since the Gouy phase accumulation is very close to zero.

The pros and cons of both designs (stable and marginally-stable) have been considered and investigated; they are described in Ref. [26]. The primary feature favoring the stable design is greater tolerance to distortions or defects in the optics. A modal model treatment of some of these effects can be found in Ref. [29].

3.15 Seismic Isolation

The main interferometer optics and components are mounted on in-vacuum, seismically isolated platforms (all components shown in Fig. 1, except the laser and phase modulators, are mounted on such platforms). Isolation from ground vibrations is achieved primarily by active stabilization, using low-noise sensors and force actuators, providing suppression in roughly the band from 0.1 Hz to 10-30 Hz. There are two layers of isolation:

- Hydraulic external pre-isolators (HEPI). These isolators are external to the vacuum system, and use low-noise hydraulic actuators for control in six degrees-of-freedom. This stage also provides positioning control of the optics platform, with a range of approximately 1 mm. (HEPI isolators have been installed on the LLO interferometer since 2003.)
- Internal seismic isolators (ISI). This layer is inside the vacuum chambers, and uses electro-magnetic actuators for control. For the optics platforms in the BSC chambers, there are two such stages cascaded in series, each of which is controlled in six degrees-of-freedom (DOF). For the platforms in HAM chambers, there is a single, six DOF stage.

With two ISI stages, better isolation is provided for the test masses and beamsplitter (the optics that occupy BSC chambers). The isolation needs for the auxiliary optics mounted on the HAM chamber platforms was investigated in Ref. [30]. Given this analysis, a single-stage design for the HAM platform was adopted ([37]), as a worthy trade-off of performance for simplicity.

3.16 Suspensions

Most of the in-vacuum interferometer optics and components are mounted in pendulum suspensions, which are in turn mounted to the seismic optics platforms. The suspension

designs vary, depending on performance needs and physical constraints; most are multi-stage suspensions for better isolation compared to the initial LIGO, single-stage design. In addition, the test mass suspensions include a suspended reaction mass chain adjacent to the main chain, to provide low-noise points from which control forces can be applied to the main chain. Table 4 gives a summary of the different suspension types:

Component	*Number of suspension stages*	*Fiber type*	*Noise req. @10 Hz* $m/\sqrt{Hz}$
Test masses	4	fused silica	1×10^{-19}
Reaction masses (CP, ERM)	4	steel wire	
Beamsplitter	3	steel wire	6.4×10^{-18}
Recycling cavity optics	3	steel wire	1×10^{-17}
Input mode cleaner mirrors	3	steel wire	3×10^{-15}
Output mode cleaner	2	steel wire	1×10^{-13}
Output Faraday isolator	1	steel wire	
ETM transmission monitor	2	steel wire	
IO SM/MM optics	1	steel wire	

Table 4: Summary of suspension types in the interferometer. The test mass suspensions are paired with suspended reaction mass chains and control forces are applied between the reaction and main chains. *Fiber type* refers to the fiber at the last stage of the suspension, supporting the optic. The *noise requirement @10 Hz* refers to the motion along the optic axis, including cross-coupling from the vertical direction. Complete noise requirements for the cavity optic suspensions are given in Ref. [31]. *IO SM/MM optics* refers to steering mirrors and mode matching optics between the input mode cleaner and the PRM.

Test Mass Monolithic Suspension. The test masses will be suspended from the quad suspension penultimate mass using glass fibers (four fibers per test mass). Glass is used because its mechanical loss is several orders of magnitude smaller than that of steel and thus can give much lower thermal noise. Its high strength and low density also mean that the vertical eigenmode of the last suspension stage (aka the 'bounce mode') and the fundamental violin mode of the fibers are at lower and higher frequencies, respectively, than a corresponding steel wire suspension, thus encroaching less on the GW band.

The geometry of the glass fibers was changed in 2008 from a ribbon design (i.e., an approximately rectangular cross-section, with a 10:1 aspect ratio) to a stepped circular design [32], [33]. In this design, short sections at the ends of each fiber – i.e. the regions where the dissipation that leads to suspension thermal noise occurs – have a diameter that is chosen so that the thermally driven dimensional changes due to α and dY/dT essentially cancel each other[2]. This diameter is about twice as large as would be needed for strength alone. The diameter of the main (middle) section of fiber is kept small to maintain the low vertical mode and high violin mode frequencies.

[2] α being the thermal expansion coefficient and Y the Young's modulus

To preserve the low mechanical loss of the test mass and glass fibers, the last stage of the suspension (penultimate mass and below) is made entirely of glass: glass interface 'ears' are bonded to flats on the barrels of the test mass and penultimate mass, and the glass fibers are welded to these ears. The ear-to-mass bonds are made with hydroxide-catalysis bonding. Mechanical loss associated with these bonds has been studied [34], and these results are factored in to the interface design so as to not impact the test mass thermal noise. On the other hand, the noise associated with the monolithic suspension – i.e., the absence (or not) of excess noise in the bonds, fibers, or welds – has not been verified at the required noise level; this represents a remaining performance risk in the suspension design.

Actuation. All of the multi-stage, core optic suspensions are required to have actuation at each suspension stage for interferometer global control. At each stage, the actuation must be capable of controlling the longitudinal position and the pitch and yaw orientiation of the optic.

Direct actuation on the test masses will be made with electro-static actuators on their reaction masses. Magnetic actuators directly on the test masses are avoided to eliminate direct magnetic field noise coupling. The test mass electro-static drive (ESD) must also be able to control longitudinal position, pitch, and yaw. The ESD actuators should be made as large as possible, as dictated by the required optical apertures in the recycling cavities (for the ITMs) and for the arm transmitted beams (for the ETMs).

All other suspension types and stages (other than the test mass stages) may use magnetic actuation. The strength of the magnets used for these actuators is limited, from a noise perspective, by coupling to fluctating magnetic fields; refer to Ref. [35] for an analysis of this coupling and its implications for the quad suspension. To avoid Barkhausen noise in the magnets, somarium cobalt magnets should be used in all places where dynamical control signals are applied ([36]).

3.17 Thermal Effects and Compensation

As in initial LIGO, the interferometers will include active thermal compensation (though this time it is designed in from the beginning). The scheme used for initial LIGO, however, where a compensating CO_2 laser beam shines on the high-reflectivity side of the ITMs, does not scale well to Advanced LIGO. Furthermore, it is not just substrate thermal lensing that must be compensated. With the higher powers and near-concentric arm cavities of Advanced LIGO, thermo-elastic deformation of the test mass surfaces becomes significant as well.

The compensation scheme is therefore significantly different: a radiative ring heater will surround each test mass, and a compensation plate is included in each arm of the Michelson, suspended between the beamsplitter and each ITM. The test mass ring heaters can maintain the radii of curvature constant (keeping the cavity mode constant); they also provide some amount of thermal lens compensation. The compensation plates (CPs) are actuated on with CO_2 laser beams for additional, more flexible thermal lens compensation [24]; the CPs have the advantage of being less sensitive to actuator laser noise than direct test mass actuation.

Diagnostic sensors will independently measure thermal distortions in specific optical paths

or surfaces. Specifically, low-power laser beams (at wavelengths other than 1064 nm) probe separately the optical path of each ITM-CP pair and each ETM. Changes in the spatial wavefront of the probe beams will be monitored with Hartmann sensors.

3.18 Arm Length Stabilizer

In order to facilitate lock acquisition of the interferometers, Advanced LIGO includes an Arm Length Stabilization (ALS) system. The function of the ALS is to control the length of each arm cavity, independently of the rest of the interferometer. Each arm length is to be stabilized by the ALS to a residual fluctuation level of 1 nanometer or less. Furthermore, one will be able to set each arm to a determined microscopic length, typically so that the main laser beam is a few linewidths from resonance at the start of the acquisition procedure. More details on how the ALS is used for interferometer lock acquisition can be found in Ref. [50].

The ALS will be implemented on each arm cavity by reflection-locking from the end test masses. A 532 nm laser source at each end station is injected into the arm through the ETM, and the PDH error signal is used to stabilize the arm length. The frequency of the 532 nm source will be synchronized to the main laser frequency, with the frequency difference being controllable to set the microscopic length of the arm. The requirements and design of the ALS system are found in Refs. [51] and [52].

The ALS scheme requires the test mass dielectric coatings to be dichroic. The ETM must be partially transmissive for 532 nm and a high-reflector for 1064 nm, whereas the ITM is the reverse – a partial transmitter for 1064 nm and a high-reflector for 532 nm.

3.19 Parametric Instabilities (PI)

Opto-mechanical parametric couplings in the arm cavities have the potential to lead to unstable build-up of such coupled, higher-order modes. Unchecked, the mechanism would impose a limit on the power stored in the arms. The mechanical side of the effect involves acoustic modes of the test masses; the optical side involves higher-order spatial eigenmodes of the arm cavities. Under certain conditions, the two types of modes can non-linearly feed energy into each other, removing it from the main carrier mode.

The signifigance of the effect was first recognized by the Braginsky group [38], and the first detailed analyses for Advanced LIGO cavities were done by the University of Western Australia group [39],[40]. The general conclusion of these and other analyses (see in particular Refs. [41], [42], [43], and [44]), is that there may be 5-10 modes per test mass that could become unstable. Recently the aLIGO System has observed PI ([45]).

Several methods of mitigating parametric instabilities have been suggested and assessed to varying degrees:

1. use the thermal compensation actuators to slightly change the radius of curvature of one or more test masses; this would shift the eigen-frequency of the higher-order optical mode to avoid overlap with the corresponding acoustic mode;

2. active mode damping via the electro-static actuators,

3. application of passive, tuned dampers to the test mass;

4. active mode damping via radiation pressure from additional laser beams;

5. reduction of optical gain by restricting the test mass apertures.

The first two approaches listed above can be implemented in aLIGO without hardware changes. In fact the first approach, using the ring heater to shift the optical modes, has been sucessfully employed in aLIGO ([45]). However while this approach will allow for an increase in the power level, it is unlikely to allow aLIGO to achieve the its maximum power level. The other more promising approaches are under active investigation, but are outside the scope of the aLIGO project. Reference [46] summarizes our knowledge of and approach to parametric instabilities for Advanced LIGO.

3.20 Electro-Static Charge Control

Electro-static charge buildup on the test mass or nearby dielectrics could result in excess displacement noise via the following mechanisms:

1. charge that has a finite decay time, creating a fluctuating force via interaction with nearby charges (either real or image) [47]

2. charge that produces a fluctuating force via their motion relative to the test mass [48]

3. stationary charge which produces fluctuating force on the test mass due to varying electro-magnetic fields in the vicinity (e.g. ring heater current fluctuation)

A purely stationary (static) charge would also introduce time-invariant (static) forces on the test mass, though this is less of a concern (the static forces can be compensated). However if the residual static charge is high then the range (control authority) of the electro-static actuator will be reduced. Furthermore if the static charge is (slowly) time-varying, then compensation would need to be routinely revised, leading to an operational burden. Modeling, coupled with measurements and estimates of charge buildup mechanisms and decay time, suggest that charge noise should lie at or below the technical noise limit for Advanced LIGO.

There are four potentially significant sources, or mechanisms, for charging the test mass optics:

1. Ion pump UV and/or soft x-ray emission: In order to address ETM ionization from the ion pump, the existing end station ion pumps will be kept off, a new ion pump will be installed a considerable distance (280 m) from the ETM onto a port along the beam tube (with a chevron baffle) and a NEG pump will be added to the end station. Chevron baffling on the corner station ion pumps (distant from the ITMs) will also be employed.

2. Residual (negative) charge from First Contact removal: In order to address the residual ionization from First Contact removal, a discharging procedure (E1300017) has been put into place using an ion gun and a sensitive electrometer.

3. Air flowing past the test masses during the pump down may also cause charging.

4. Charge transfer from earthquake stop contact to the test mass: The earthquake stops have been designed to limit contact charge transfer.

Reference [49] summarizes our assessment of charge control in Advanced LIGO. The issue continues to be investigated within LIGO and the LSC.

Based upon initial operational experience it seems clear that we need a means of discharging the TMs, regardless of the charging source. The prototype system for discharging the TMs has been successfully tested at LASTI and LHO. (Recent testing with this prototype at LLO have been less successful; Charge on the back face of the TM (in the narrow gap to the RM) has not been completely discharged and is the subject of continued testing.) The Test Mass Discharging System (TMDS) injects equal amounts of positively and negatively ionized, clean, dry gas into the TM chamber. A production version of the TMDS is being fabricated by the project and will be delivered in sufficient quantity to outfit all TM chambers.

4 System Level Noise Sources

4.1 Fundamental noise sources

The interferometer noise floor is designed to be limited by fundamental noise source – quantum noise and thermal noise. While these arise from fundamental physical mechanisms and cannot be 'engineered away', they depend on parameters that can be controlled to some degree. This section shows the equivalent strain noise due to these sources (see Fig. 3), and describes the current parameter values that are used in the calculations.

GWINC The noise sources are calculated using GWINC (Gravitational Wave Interferometer Noise Calculator), a collection of matlab functions that contain mostly analytical formulations of the noise phenomena [54]. GWINC also calculates the sensitivity of a given design to different astrophysical sources of GWs. All strain noise plots and source sensitivities given in this document were calculated with version v3 of GWINC, with one caveat regarding the suspension thermal noise, as explained in Sec. 4.1.3.

4.1.1 Quantum noise

For a given stored power in the arm cavities, the quantum noise spectrum is affected in detail by the signal recycling mirror reflectivity, loss in the signal recycling cavity, and the photodetector quantum efficiency. GWINC uses the detailed quantum noise formulation of Buonanno and Chen found in Section V of Ref. [55]; these expressions account for loss in the signal cavity and the detector efficiency.

The following values are used for the loss parameters: 90% for the photodetection efficiency (this accounts for finite transmission through the Faraday isolator and output mode cleaner, as well as photodetector quantum efficiency); 2000 ppm for the round-trip loss in the signal recycling cavity. Figure 4 shows the quantum noise component for each of the modes described

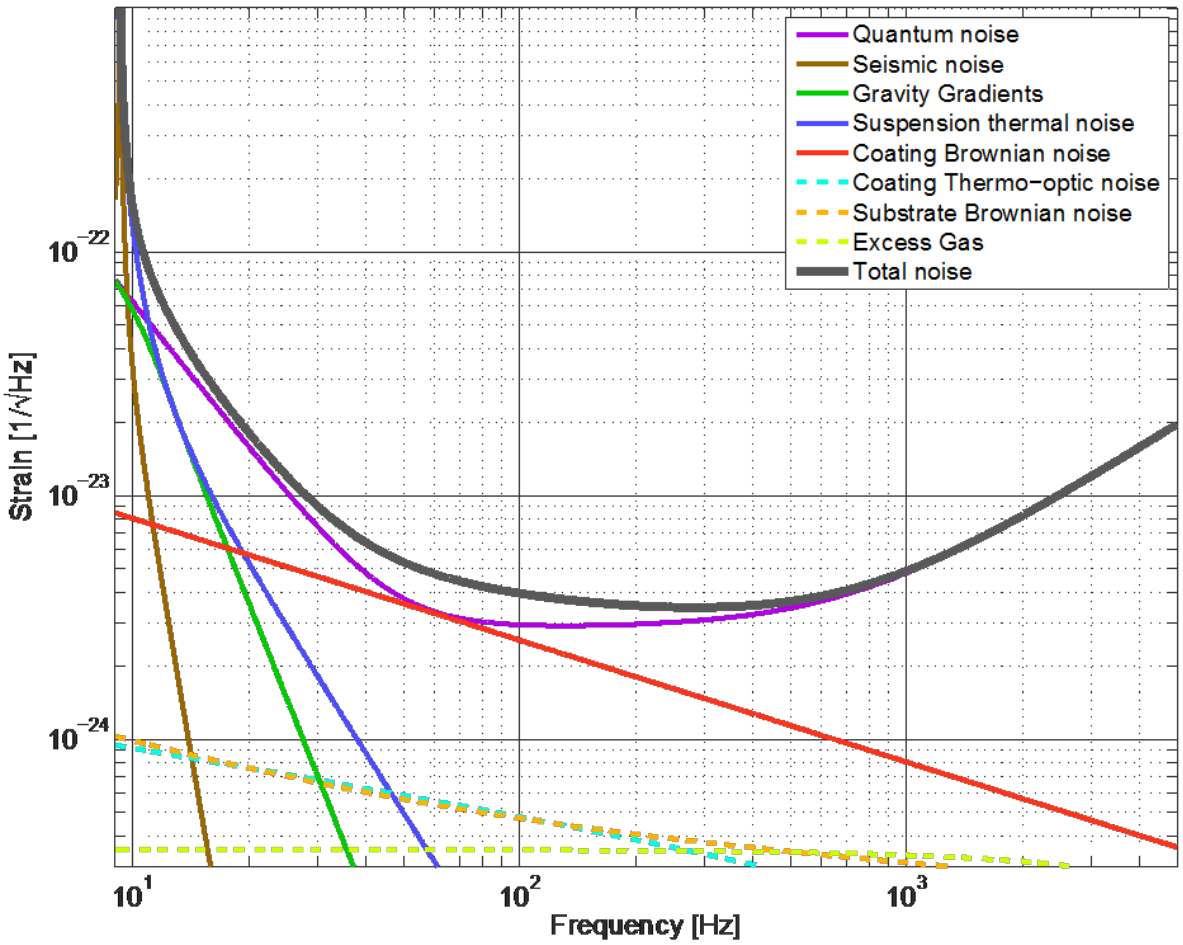

Figure 3: Fundamental noise sources for broadband, high power operation – Nominal mode of Fig. 2, with 125 W of input power.

in Section 3.1. It also shows quantum noise for a mode tuned for binary black hole inspsirals, and a high-frequency, narrowband mode, which requires a signal recycling mirror with a much smaller transmission (1.1%).

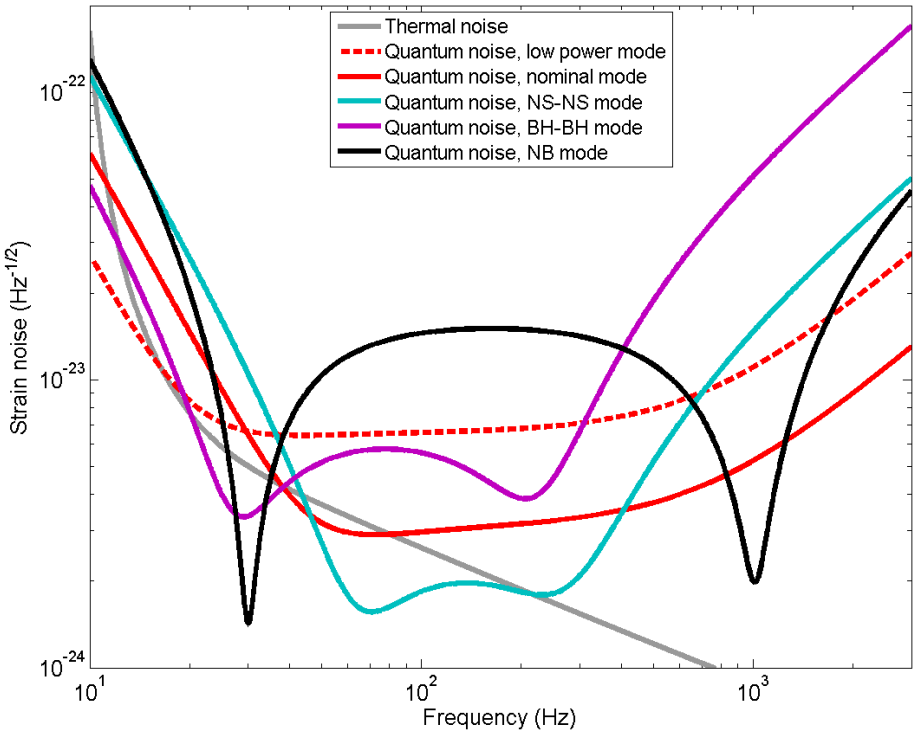

Figure 4: Quantum noise for the modes described in Section 3.1, as well as two additional modes (of more specialized interest): a mode tuned for detection of an inspiral of two 30-solar-mass black holes (BH-BH); a narrowband mode where the signal recycling mirror is changed for one with much smaller transmission (1.1% vs. 20%). Total thermal noise (suspension and test mass) is also shown for comparison.

4.1.2 Test mass internal thermal noise

The test mass internal thermal noise is calculated with the following components:

1. *Substrate Brownian noise.* Noise due to bulk mechanical loss is calculated according to Ref. [56], which includes finite size corrections. Surface loss is also included in the same way that coating loss is calculated. The bulk and surface loss model used in the calculation is that of Ref. [57].

2. *Substrate thermoelastic noise.* This is the noise from thermal fluctuations acting via the thermal expansion coefficient of the test mass substrate. It is also calculated according to Ref. [56] and is included in the total noise, but it is much smaller than the substrate Brownian noise and not shown in Fig. 3.

3. *Coating Brownian noise.* This is the noise due to mechanical dissipation in the coatings, and is calculated according to the formulation in Ref. [58]. This calculation does not account for the finite size of the test mass. An analytic formulation of coating thermal noise in a finite-sized mirror has been done recently ([22]), with the finding that for Advanced LIGO mirror parameters, the effect of the finite size is very small – the finite size calculation gives a displacement noise, at 100 Hz, that is about 3% smaller than the infinite-approximation result.

4. *Coating thermo-optic noise.* Coating thermo-optic noise is that which arises from thermal dissipation in the coatings, producing noise via the thermoelastic and thermorefractive mechansisms. It is calculated in a coherent manner according to Ref. [59].

Coating Brownian noise is the dominant of these terms. The test mass thermal noise shown in Fig. 3 is calculated using the parameters in Table 5.

Parameter	*Value*	*Ref.*
fused silica bulk loss	$7.6 \times 10^{-12} f^{0.77}$	[57]
low-index coating material (silica)		
mechanical loss	4×10^{-5}	G0900216
thermal expansion	$5.1 \times 10^{-7}/K$	[60]
index of refraction	1.45	
dn/dT	$8 \times 10^{-6}/K$	[61]
Young's modulus	72×10^{9} Pa	[60]
layer optical thickness, ITM / ETM	$0.308\,\lambda$ / $0.27\,\lambda$	
high-index coating material (doped tantala)		
mechanical loss	2.3×10^{-4}	[62]
thermal expansion	$3.6 \times 10^{-6}/K$	[60]
index of refraction	2.0654	
dn/dT	$1.4 \times 10^{-5}/K$	G0900224
Young's modulus	140×10^{9} Pa	[60]
layer optical thickness, ITM / ETM	$0.192\,\lambda$ / $0.23\,\lambda$	
optical transmission, ITM / ETM	1.4% / 5 ppm	

Table 5: Significant parameters that determine the test mass internal thermal noise.

4.1.3 Suspension thermal noise

A description of the calculation used in GWINC (v3) for suspension thermal noise can be found in section 2.3 of Ref. [64]. It models the four stages of the suspension as point masses connected by springs. Dissipation in each stage is included as imaginary parts of the spring constants, including loss terms for bulk loss, surface loss, and thermoelastic damping. The thermal noise in the detection band is of course dominated by loss in the final suspension stage, which is calculated following Ref. [65].

However, the GWINC formulation is not able to handle the stepped circular geometry of the actual suspension fiber design. Suspension thermal noise is calculated instead with the Mathematica-based model of M Barton [66]. For all the plots and figures-of-merit in this document, the output of this model[3] is substituted for the GWINC suspension thermal noise. The M. Barton model does not include the violin modes of the fibers, so these do not show up in the plots. The fundamental violin mode will be at approximately 500 Hz. Parameter values significant to the thermal noise calculation are given in Table 6.

Parameter	*Value*	*Ref.*
Total length	60.2 cm	
Diameter, central region	$400\,\mu m$	
Diameter, end sections	$800\,\mu m$	
Length of each end section	1.5 cm	
Heat capacity	$770\,\mathrm{J/kg/^\circ K}$	[67]
Thermal conductivity	$1.38\,\mathrm{W/m/kg}$	[67]
Thermal expansion coeff.	$3.9 \times 10^{-7}/^\circ\mathrm{K}$	[68]
Young's modulus (E)	7.2×10^{10} Pascals	[67]
Temperature coeff. of E	$(1/E)dE/dT = 1.52 \times 10^{-4}/^\circ\mathrm{K}$	[68]
Effective structural loss	1.2×10^{-7}	[57]

Table 6: Significant parameters of the test mass suspension glass fibers that determine suspension thermal noise.

4.2 Facility limits

4.2.1 Seismic gravity-gradient noise

Seismic waves produce density perturbations in the earth close to the test masses, which in turn produce fluctuating gravitational forces on the masses. This noise source is called seismic gravity-gradient noise, and is estimated using the transfer function formulation of Ref. [69]. This requires a model for the spectrum of rms seismic displacements averaged over vertical and horizontal directions ($W(f)$), and an estimate of a dimensionless reduced transfer function (β). We use a value of $\beta = 0.6$, compared to a total range found in Ref. [69] of $\beta = 0.15 - 1.4$. The model for $W(f)$ is shown in Fig. 5.

4.2.2 Residual gas noise

Optical path length noise due to residual gas in the beam tubes is calculated using the equation found in Ref. [70]. The calculation accounts for the changing beam size over the path along the arm. The noise curve includes only the dominant residual gas component, hydrogen, with a pressure of 4×10^{-7} pascals (polarizability of $7.8 \times 10^{-31}\,\mathrm{m}^3$).

[3] specifically, file QuadLite2Lateral_mark_barton_20120601TMproductionTM_TN.m is used (naming convention of M. Barton)

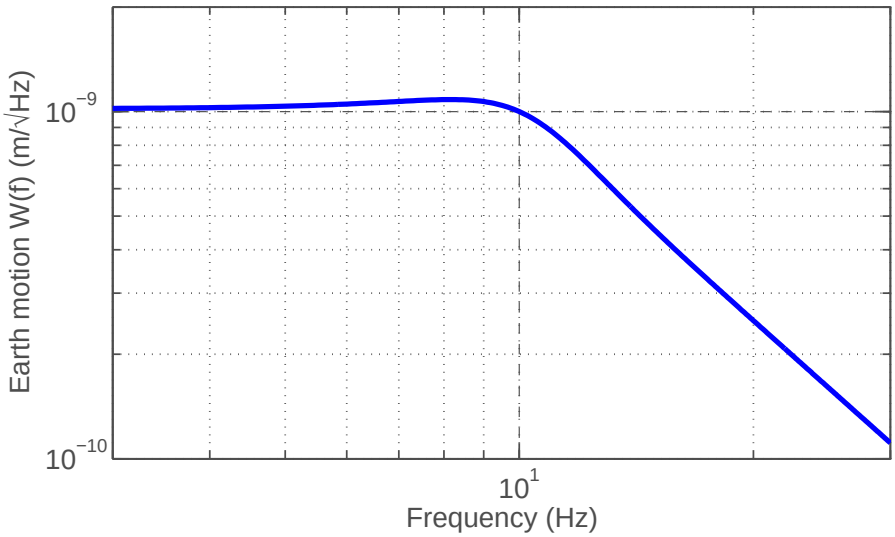

Figure 5: Model used for the rms seismic displacement in the gravity-gradient noise estimate, averaged over horizontal and vertical directions (the motion spectrum $W(f)$ as defined in Ref. [69]).

4.3 Technical noise sources

All technical noise sources are to be controlled so that the equivalent strain noise (amplitude spectral density) of each source is no more than 10% of the target strain sensitivity. This applies across the entire gravitational wave band (10 – 7000 Hz). Since the different operating modes have different strain noise floors, for guidance we form a technical noise floor by using the minimum strain noise amongst the modes at each frequency; this is shown in Fig. 6, now displayed as equivalent differential-arm displacement noise. For some noise sources (particularly those that depend on power) this may be overly conservative; in these cases the technical noise limit can be calculated specifically for that situation.

5 Subsystems

5.1 Prestabilized laser

The PSL subsystem includes:

- Nd:YAG laser, 1064 nm wavelength, single frequency, TEM_{00} mode output power of 165 W.
- frequency prestabilization of the PSL output beam
- intensity stabilization of the input mode cleaner output beam
- frequency actuation inputs, for subsequent frequency control
- amplitude and frequency modulation inputs, for global diagnostics

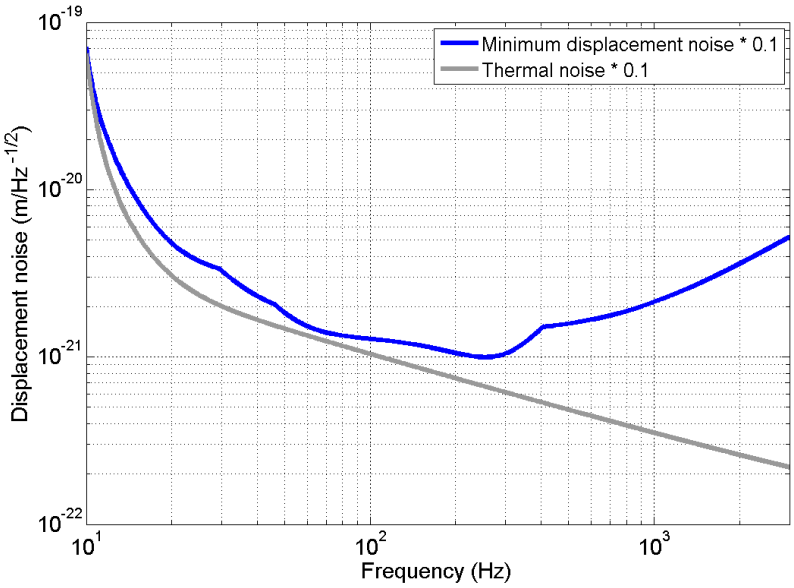

Figure 6: Equivalent differential-arm displacement noise limit for technical noise sources. The blue curve is 10% of the minima of the curves shown in Fig. 2 (converted to displacement by multiplying by the arm length). Displacement noise limit for a single test mass would be a factor of 2 smaller. For reference, the grey curve is 10% of the thermal noise (sum of suspension and test mass internal noise).

The PSL document tree starts at LIGO-E1200480.
The PSL design requirements document is LIGO-T050036.
The PSL final design document is LIGO-T0900649.
The PSL acceptance review documentation is linked at LIGO-E1200038.

5.2 Seismic isolation

The seismic isolation subsystem (SEI) includes:

- Hydraulic external pre-isolators (HEPI) for all BSC chambers, and all HAM chambers except HAM1 and HAM7.
- Single-stage active isolation platform for all HAM chambers, except HAM1 (known as the HAM - Internal Seismic Isolation (HAM-ISI).
- Two-stage active isolation platform for all BSC chambers (known as the BSC-ISI).

General requirements for the seismic isolation system, and displacement noise requirements for the BSC platforms are found in LIGO-E990303. Displacement noise requirements for the HAM platforms are found in LIGO-T060075.

The SEI document tree starts at LIGO-E1200684.
The overall SEI design requirements document is LIGO-E990303. The displacement noise

requirements for the non-SRC, HAM-ISI platforms are defined in LIGO-T060075. The displacement noise requirements for the SRC HAM-ISI platforms (HAM4 and HAM5) are defined in LIGO-T1000216.
The HAM-ISI final design document is LIGO-E1500044. The BSC-ISI final design document is LIGO-L0900222. The HEPI fabrication readiness review is documented in LIGO-M080113. The SEI acceptance review documentation is linked at LIGO-E1200038.

5.3 Input optics

The input optics (IO) subsystem includes:

- electro-optic modulators for the interferometer sensing scheme
- input mode cleaner design
- mode matching elements between the input mode cleaner and the power recycling mirror
- cavity mode design for the power- and signal-recycling cavities (mirror radii of curvature and separations)
- power control of the beam incident on the input mode cleaner
- delivery of the interferometer reflected beam, the input mode cleaner reflected beam, and a sample of the IMC transmitted beam to detection ports
- Faraday isolator between the IMC and the power recycling mirror
- ensure the required level of input beam pointing stability
- beam dumps and stray light baffles in the IO section of the vacuum system

The IO document tree starts at LIGO-E1200584.
The IO design requirements document is LIGO-T020020.
The IO final design document is LIGO-T0900386.
The IO acceptance review documentation is linked at LIGO-E1201013.

5.4 Core optics

The scope of the core optic components (COC) subsystem includes:

- procurement of the following interferometer optics, including all coatings applied to them: test masses; end reaction masses; compensation plates; beamsplitter; fold mirrors; the large optics in the recycling cavities
- metrology of all core optics
- specification of cleaning procedures for core optics

The COC document tree starts at LIGO-E1200484.
The COC design requirements document is LIGO-T000127.
The COC final design document is LIGO-E080494.
The COC acceptance review documentation is linked at LIGO-E1300769.

5.5 Suspensions

The suspensions subsystem (SUS) includes:

- suspension mechanics for all core optics, for the small optics in the recycling cavities, for the input mode cleaner optics, and for the output mode cleaner
- local sensors, actuators and controls for local damping of these suspensions
- actuators and actuator-drivers for global control of suspended optics

The suspensions design requirements are found in LIGO-T010007.

The SUS document tree starts at LIGO-E1200482.
The primary SUS design requirements documents are LIGO-T000053 and LIGO-T010007.
The SUS final design documentation is summarized in LIGO-T1200463.
The SUS acceptance review documentation is linked at LIGO-E1400019.

5.6 Interferometer sensing & control

The interferometer sensing and control (ISC) subsystem includes:

- design of the interferometer sensing scheme
- sensors and controls for maintaining the interferometer lengths and alignment during operation
- sensors and controls for stabilizing the length and alignment of the input mode cleaner
- interferometer lock acquisition: hardware and/or algorithms for achieving the operating point of the interferometer
- signal sources for modulation frequencies used in the sensing scheme
- the in-vacuum optics platform and any seismic isolation of the platform for the input HAM chamber (HAM1/HAM7)
- any outside-the-vacuum mounting platforms for ISC hardware

The ISC document tree starts at LIGO-E1200122.
The ISC design requirements document is LIGO-T070236.
The ISC final design documentation is listed within the final design review report, LIGO-T1000334.
The ISC acceptance review documentation is linked at LIGO-E1300833.

5.7 Auxiliary optics support

The auxiliary optics support (AOS) subsystem includes:

- Initial Alignment System (IAS): surveying support for proper installation of components
- Photon calibrators (PCal): calibration tool using photon pressure of a modulated laser beam
- Optical levers (OptLev) to monitor orientation of suspended optics relative to the floor
- In-vacuum stray light control (SLC): baffles and beam dumps for diffuse scattering and ghost beams; Viewports for beams entering and exiting the vacuum system; an Output Faraday Isolator (OFI, in-vacuum) for the anti-symmetric port output beam
- Beam reducing telescope and suspension for the ETM transmission monitor (TMS)
- Thermal compensation system (TCS): senses thermal distortions of core optics and corrects by adding compensating heat
- Video cameras for monitoring beam positions and sizes on the core optics

The AOS document tree starts at LIGO-E1200481.

Sub-subsystem	*DRD*	*FDD*	*Acceptance*
IAS	T080307	T1000230	E1300547
PCal	T1100044	T1100068	T1400283
OptLev	T0900174, T1000132	E1200030	E1200026
SLC	T070061, T1000022	VP: T1000746	T1400233
		OFI: T1000181	
		SRC Baffles: T1100445	
		Manifold/Cryopump, MCT Baffles: T1100165	
		ITM Elliptical Baffles: T1100446	
		BS Elliptical Baffles: T1200313	
TMS	T0900265	E1100537	T1400282
TCS	T000092	CO2P: T1100570	E1300799
		HWS: T1100517	E1300802
		RH: R1000837	E1300892

Table 7: AOS design documentation.
DRD = design requirements document; FDD = final design document; MCT = mode cleaner tube; CO2P = CO_2 laser projection system; HWS = Hartmann wavefront sensor; RH = ring heater

5.8 Control and data system

The control and data systems (CDS) infrastructure includes:

- Data Acquisition (DAQ) System
- Timing and Synchronization System
- Computer Networking Systems
- Control room computer systems
- Diagnostic Monitoring Tool (DMT) computers

The CDS document tree starts at LIGO-E1200645.
The CDS design requirements document is LIGO-T070056.
The CDS final design documentation is listed within the final design review report, LIGO-T080243.
The CDS acceptance review document is LIGO-E1300536.

References

[1] *aLIGO System Acceptance Document*, LIGO-E1400371

[2] *Advanced LIGO*, LIGO-P1400177

[3] *Technical Review Board (TRB) Report: Recommendation regarding which Interferometer (H1 or H2) to Offer to LIGO-India*, LIGO-L1200053-v3.

[4] *Advanced LIGO Project Execution Plan*, LIGO-M050303

[5] *Advanced LIGO Reference Design*, LIGO-M060056

[6] *LIGO Science Requirements Document (SRD)*, LIGO-E950018

[7] *aLIGO Availability Estimate*, LIGO-E1400310

[8] *Optimal calibration accuracy for gravitational-wave detectors*, Lindblom L 2009 Phys. Rev. D 80 042005.

[9] *RODA: Increase of Schnupp Asymmetry from 5 cm to 8 cm*,LIGO-M1200276

[10] *aLIGO Interferometer Optics Positions and Orientations for Initial Alignment*, D. Coyne, LIGO-E1300128.

[11] *Optical Layout and Parameters for the Advanced LIGO Cavities*, M. Arain and G. Mueller, LIGO-T0900043

[12] *DC Readout Experiment in Enhanced LIGO*, T. Fricke, et. al., CQG 29 (2012) 065005 (18pp), LIGO-P1000009

[13] *DC Readout for Advanced LIGO*, P. Fritschel, LIGO-G030460

[14] *Quantum noise in laser-interferometer gravitational-wave detectors with a heterodyne readout scheme*, A. Buonanno, Y. Chen, N. Mavalvala, Phys.Rev. D67 (2003) 122005.

[15] *DC Readout Experiment at the Caltech 40m Prototype Interferometer*, R. Ward, et. al., Class Quant Grav vol. 25 pg. 114030 (8pp)., LIGO-P070125.

[16] *Balanced Homodyne Readout for Quantum Limited Gravitational Wave Detection*, P. Fritschel, M. Evans, V. Frolov, Opt Express. 2014 Feb 24;22(4):4224-34, LIGO-P1300184.

[17] *Optical torques in suspended Fabry-Perot interferometers*, J. Sidles and D. Sigg, Phys. Lett. A, 354 (2006) 167.

[18] *Arm Cavity Finesse for Advanced LIGO*, P. Fritschel, R.Adhikari, S. Ballmer, M. Evans, `http://www.ligo.caltech.edu/docs/T/T070303-01.pdf`

[19] *Advanced LIGO Substrate Selection Recommendation*, `http://www.ligo.caltech.edu/docs/M/M040405-00/M040405-00.pdf`

[20] *Test Mass Material Down-select Plan*, `http://www.ligo.caltech.edu/docs/T/T020103-08.pdf`

[21] *Dimensions for Advanced LIGO Fused Silica Test Masses*, P. Fritschel, `http://www.ligo.caltech.edu/docs/T/T040199-00.pdf`

[22] *Coating thermal noise of a finite-size cylindrical mirror*, K. Somiya, K. Yamamoto, Phy Rev D, 79, 102004 (2009), LIGO-P080121.

[23] *Titania-doped tantala/silica coatings for gravitational-wave detection*, Harry G M et al 2007 Class. Quantum Grav. 24 405415, LIGO-P050048.

[24] *TCS and the Golden Shield*, M. Evans and P. Fritschel, LIGO-T0900359.

[25] *Core Optics Components (COC) Design Requirements Document (DRD)*, LIGO-T000127.

[26] *Stable Recycling Cavities for Advanced LIGO*, P. Fritschel, H. Yamamoto, G. Mueller, M. Arain, LIGO-T080208.

[27] *Interferometer Sensing and Control Design Requirements*, R. Adhikari, S. Ballmer, P. Fritschel, LIGO-T070236.

[28] *Pre-Stabilized Laser Design Requirements*, B. Willke, P. King, R. Savage, P. Fritschel, LIGO-T050036.

[29] *Optimal degeneracy for the signal-recycling cavity in Advanced LIGO*, Yi Pan, `http://arxiv.org/pdf/gr-qc/0608128`.

[30] *HAM Seismic Isolation Requirements*, P. Fritschel, `http://www.ligo.caltech.edu/docs/T/T060075-00.pdf`

[31] *Cavity Optics Suspension Subsystem Design Requirements Document*, LIGO-T010007.

[32] *Development of Fused Silica Suspensions for Advanced Gravitational Wave Detectors*, A. Heptonstall, talk given at the March 2008 LSC meeting, Caltech, Pasadena, CA.

[33] *RODA: ETM/ITM suspensions to use tapered circular cross-section silica fibre*, LIGO-M080363.

[34] *Thermal noise arising from bonds in the Advanced LIGO test mass suspensions*, L. Cunningham et al., LIGO-P0900052.

[35] *Considerations regarding magnet strengths for the Advanced LIGO test mass quadruple suspensions*, P. Fritschel, `http://www.ligo.caltech.edu/docs/T/T050271-00.pdf`

[36] *RODA: Magnet sizes and types and OSEM types in Adv. LIGO suspensions*, LIGO-M0900034.

[37] *HAM Single-Stage Isolation Baseline Option Review Report*, F. Raab, `http://www.ligo.caltech.edu/docs/M/M060062-00/M060062-00.pdf`

[38] *Parametric oscillatory instability in FabryPerot interferometer*, V. B. Braginksy, S. Strigin, and S. Vyatchanin, Phys. Lett. A 287, 331 (2001).

[39] *Parametric Instabilities and Their Control in Advanced Interferometer Gravitational-Wave Detectors*, C. Zhao et al., Phys. Rev. Lett. 94, 121102 (2005).

[40] *Multiple modes contributions to parametric instabilities in advanced laser interferometer gravitational wave detectors*, L. Ju et al., Phys. Lett. A 354, 360 (2006).

[41] *Investigating a Parametric Instability in the LIGO Test Masses*, H. Bantilan and W. Kells, `http://www.ligo.caltech.edu/docs/T/T060207-00/T060207-00.pdf`.

[42] *Ring Dampers and Gold Coatings*, C. Zhao, talk given at the March 2008 LSC meeting, Caltech, Pasadena, CA.

[43] *A General Approach to Optomechanical Parametric Instabilities*, M. Evans, L. Barsotti and P. Fritschel.

[44] *Monte Carlo simulation of Parametric Instabilities in aLIGO*, S. Gras, LIGO-G1401131.

[45] *Observation of Parametric Instability in Advanced LIGO*, M. Evans, et. al., draft paper in preparation for publication, LIGO-P1400254.

[46] *Review of the parametric instability problem in Advanced LIGO*, P. Fritschel, M. Evans, LIGO-T0900437.

[47] *Estimate of Noise from Charging in Initial, Enhanced, and Advanced LIGO*, G. Harry, editor, LIGO-T080019.

[48] *Simple Calculations of Charge Noise for Advanced LIGO*, B. Lantz, LIGO-T080214.

[49] *Charging status presentation to systems group*, R. Weiss, LIGO-G1401153.

[50] *AdvLIGO Interferometer Sensing and Control Conceptual Design*, LIGO-T070247

[51] *Adv. LIGO Arm Length Stabilisation Requirements*, LIGO-T0900095.

[52] *Adv. LIGO Arm Length Stabilisation Design*, LIGO-T0900144.

[53] `http://ilog.ligo-wa.caltech.edu:7285/advligo/Seismic_Platform_Interferometer`

[54] GWINC is derived from Bench, and is kept in a CVS repository hosted at MIT. It was re-named from Bench in 2008, when its structure was changed to make it more modular and it was put under CVS control. It can be accessed from the Advanced LIGO wiki: `https://awiki.ligo-wa.caltech.edu/aLIGO/GWINC`

[55] *Quantum noise in second generation, signal-recycled laser interferometric gravitational-wave detectors*, A. Buonanno and Y. Chen, Phys.Rev. D64 (2001) 042006.

[56] *Thermoelastic Noise and Homogeneous Thermal Noise in Finite Sized Gravitational-Wave Test Masses*, Y. Liu, K. Thorne, Phys.Rev. D62 (2000) 122002.

[57] *Frequency and Surface Dependence of the Mechanical Loss in Fused Silica*, S. Penn et al., Phys. Lett. A 352 (2006) 3.

[58] *Optical coatings for gravitational-wave detection*, G. M. Harry et al., Proceedings of SPIE: 5578 (SPIE, Bellingham, WA, 2004).

[59] *Thermo-optic noise in coated mirrors for high-precision optical measurements*, M. Evans et al., Phys. Rev. D 78 (2008) 102003.

[60] *Thermoelastic dissipation in inhomogeneous media: loss measurements and displacement noise in coated test masses for interferometric gravitational wave detectors*, Fejer et al., Phys. Rev. D 70 (2004) 082003.

[61] *Active Wavefront Correction in Laser Interferometric Gravitational Wave Detectors*, R. Lawrence, Ph.D. thesis, M.I.T., 1997. Note: the bulk value of dn/dT is being used.

[62] *Comparison of the temperature dependence of the mechanical dissipation in thin films of Ta2O5 and Ta2O5 doped with TiO2*, I. W. Martin et al., Class. Quant. Grav. 26 (2009) 155012.

[63] *Optimized multilayer dielectric mirror coatings for gravitational wave interferometers*, J. Agresti et al., Proceedings of the SPIE, Volume 6286, pp. 628608 (2006).

[64] *Advanced LIGO Suspension System Conceptual Design*, N. Robertson et al., `http://www.ligo.caltech.edu/docs/T/T010103-05.pdf`.

[65] *Dissipation of mechanical energy in fused silica fibers*, A. Gretarrson and G. Harry, Rev. Sci. Instrum. 70 (1999) 4081.

[66] *Models of the Advanced LIGO Suspensions in Mathematica*, M. Barton, LIGO-T020205-02, in conjunction with the bug fix described in T0900320-v1.

[67] Fused silica properties from Heraeus, available through www.heraeus-quarzglas.com

[68] *Investigations of the dynamics and mechanical dissipation of a fused silica suspension*, P. Willems et al., Phys. Lett. A 297 (2002) 37.

[69] *Seismic gravity-gradient noise in interferometric gravitational-wave detectors*, S. Hughes, K. Thorne, Phys. Rev. D 58 (1998) 122002.

[70] *Measurement of Optical Path Fluctuations due to Residual Gas in the LIGO 40 Meter Interferometer*, M. Zucker, S. Whitcomb, `http://www.ligo.caltech.edu/docs/P/P940008-00.pdf`.